

Electron Backscatter Diffraction Analysis for Polarization of SrBi₂(Ta,Nb)₂O₉ Ferroelectric Capacitors in Submicron Small Area

Kazuhiro KAIBARA*, Keisuke TANAKA, Kiyoshi UCHIYAMA, Yoshihisa KATO, and Yasuhiro SHIMADA

Semiconductor Devices Research Center, Semiconductor Company, Matsushita Electric Industrial Co., Ltd.,
1-1 Saiwai-cho, Takatsuki, Osaka 569-1193, Japan

(Received December 21, 2005; accepted October 19, 2007; published online January 18, 2008)

We investigate the size and crystal orientation of each small grain of ferroelectric SrBi₂(Ta,Nb)₂O₉ (SBTN) films within very small areas by an electron backscatter diffraction (EBSD) analysis technique. The obtained map of the grains reveals that the size of *c*-axis-oriented grains increases as the average grain size of the films increases. On the other hand, the size of *a*-axis-oriented grains, each of which has a finite remnant polarization normal to the films, is almost unchanged. The area fraction of the *a*-axis-oriented grains is in good agreement with the measured polarizations of ferroelectric capacitors with different average grain sizes. This result implies that an increase in the number of relatively small *a*-axis-oriented grains is effective for increasing the total polarization of the ferroelectric films. The demonstrated analysis technique is very useful for the precise design of future high-density ferroelectric random access memories (FeRAMs) with very small capacitor structures, each of which consists of only a few grains. [DOI: 10.1143/JJAP.47.262]

KEYWORDS: crystal orientation, grain size, polarization, electron backscatter diffraction (EBSD)

1. Introduction

Ferroelectric random access memories (FeRAMs) have been widely investigated as next-generation nonvolatile memories owing to the possible low power consumption, high-speed readout and high-write endurance compared with existing nonvolatile memories such as electrically erasable programmable read-only memories (EEPROMs) and flash memories.^{1,2)} By taking advantage of these superior characteristics, FeRAMs have been successfully commercialized for portable electric devices or smart cards, even though they still have a low density.

Increasing the integration density of FeRAMs would further extend the applications of FeRAMs to mobile phones, internet appliances or personal digital assistants, which would require large-scale integrated circuits (LSIs) with embedded high-density FeRAMs. Since the area of a capacitor is reduced in the high-density FeRAMs, only a few grains exist in one capacitor area of 0.1 μm². Widely used ferroelectric materials such as SrBi₂Ta₂O₉ (SBT) and SrBi₂(Ta,Nb)₂O₉ (SBTN), are anisotropic, the crystals of which are polarized only at the *a*-axis.³⁾ Thus, a variation in crystal orientation must be precisely predicted for the successful fabrication of the working high-density FeRAMs with a sufficiently high polarization for each capacitor structure. Thus, the crystal orientation has been characterized by X-ray diffraction (XRD) analysis. Bae *et al.* reported that an SBT film deposited on (111)-oriented Pt preferentially grows along the *c*-axis with a large grain size, as revealed by XRD analysis.⁴⁾ The spot size of an X-ray beam is more than 10 μm, which is much larger than the typical ferroelectric grain size. The crystal orientation measured by XRD analysis is still an average value; thus, it is not much useful for the design of a small-area capacitor with only a few grains. A detailed analysis by which the crystal orientation of each grain is revealed would be required for the design and fabrication of future high-density FeRAMs with very small capacitor structures.

In this paper, we investigate the size and crystal orientation

of each small grain in SBTN films in detail by an electron backscatter diffraction (EBSD) analysis technique^{5–8)} for the first time. On the basis of the measured distribution of the crystal orientation, the fraction of the *a*-axis orientation in the total area corresponding to the magnitude of remnant polarization is extracted. The resultant *a*-axis is in good agreement with the measured polarization of a ferroelectric capacitor, implying that the demonstrated EBSD analysis technique is viable for the precise prediction of the total polarization of such a small capacitor. It is also noted that the cross-sectional EBSD analysis of SBTN on Pt reveals in detail the distribution of the crystal orientation at the interface. This technique would be useful for the fabrication and design of future three-dimensional (3D) ferroelectric capacitors.

2. Experimental Methods

2.1 Deposition and crystal orientation of SBTN films on Pt

The SBTN films to be characterized by EBSD analysis were prepared as follows. Ti and Pt films were deposited by sputtering on thermally oxidized SiO₂ films on Si substrates. (111)-oriented Pt was deposited on SiO₂. Then 60-nm-thick SBTN films were deposited on Pt by a metal-organic chemical vapor deposition (MOCVD) technique at several pressures. Sample E was deposited at 133 Pa, and the other samples were deposited at 533 Pa. A Pt top electrode was selectively formed by electron-beam deposition over the SBTN films to measure the electrical characteristics. Then, the SBTN films were annealed by rapid thermal annealing (RTA) under several conditions, varying the temperature to change the grain size. Samples A and B were annealed by RTA with lamps set over and under the samples, and the other samples were annealed by RTA with lamps set over the samples. Sample A was annealed at 800 °C. Sample C was annealed at 750 °C. Samples B, D, and E were annealed at 785 °C. The prepared samples are labeled from A to E, the typical cross-sectional SEM image of which is shown in Fig. 1.

2.2 Determination of crystal orientation and grain size

The crystal orientation was observed using an EBSD system installed in a field emission scanning electron

*E-mail address: kaibara.kazuhiro@jp.panasonic.com

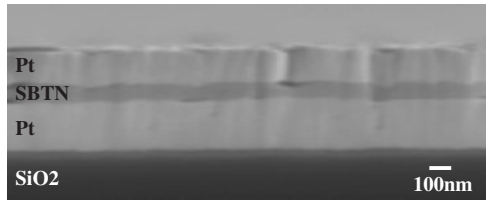


Fig. 1. Cross-sectional SEM photograph of SBTN film with thickness of 60 nm, which is sandwiched by Pt electrodes.

microscope (FE-SEM). The acceleration voltage of FE-SEM was set to be 25 kV. In an EBSD system, the electron beam irradiated on the film penetrates a region at a depth of 50 nm and scatters in all directions. Some of the backscattered electrons, which satisfy Bragg's law, diffract on lattice planes. These diffracted electrons show an EBSD pattern consisting of bright and dark lines on a phosphor screen, which are known as Kikuchi lines. The width, intensity, cross angle, and position of these Kikuchi lines are associated with the crystal structure, lattice constant and crystal orientation. Thereby, the crystal structure and lattice constant of the film must be identified prior to the determination of the crystal orientation using the EBSD pattern.

The crystal structure of the SBTN film is orthorhombic in which the difference in lattice constant between the *a*- and *b*-axes is negligibly small. Moreover, the EBSD system cannot resolve the difference in lattice constant around several picometers. Thus, we conducted EBSD characterization by assuming that the SBTN film has a tetragonal crystal structure with the same lattice constants of the *a*- and *b*-axes.

The crystal orientation of the grain is determined by the dominant axis within a solid angle of 30° centered in the normal direction of the surface. The *a*-axis-oriented grain or *c*-axis-oriented grain is defined if the dominant axis is an *a*- or *c*-axis, respectively.

The minimum spatial resolution of the present EBSD system is approximately 20 nm, which depends on the scattering area of the irradiated electron beam into the film. The irradiation of the electron beam was performed at 20° relative to the sample surface, and the scanning resolution was set to be 25 nm.

3. Results

Figure 2(a) shows the surface SEM photographs of the above-mentioned five SBTN samples with different grain sizes. The crystal orientation maps measured for the same regions are also shown in Fig. 2(b). These maps are obtained by scanning the electron beam on the sample surface and analyzing the obtained EBSD results. The crystal orientation of each point in the maps along the normal direction of the substrate is displayed using color keys; as shown in Fig. 2.

The shape of the grain, which is shown in the SEM photographs in Fig. 2(a), well agrees with the areas observed in the crystal orientation maps in Fig. 2(b), implying that the crystal orientation and grain size of individual grains can be characterized using the EBSD pattern.

In these crystal orientation maps, a red portion and a green portion represent a *c*-axis-oriented grain and an *a*-axis-oriented grain, respectively. As the average grain size increases, the *c*-axis-oriented grain size increases. On the other hand, the uniform distributions of crystal orientations are observed for small grains.

Table I shows the average sizes of all grains, *a*-axis-oriented grains, and *c*-axis-oriented grains measured using the SEM images and the EBSD results for the five samples.

Figure 3 shows the occupied areas of the *a*- and *c*-axis-oriented grains for Samples A and E as functions of grain size. In Sample A, whose average grain size is the smallest among the five samples, the crystal orientations of grains smaller than 0.2 μm² are randomly distributed. In contrast, large grains in sample E are mainly oriented to the *c*-axis, while all the *a*-axis-oriented grains are still smaller than 0.2 μm².

Table I. Average sizes of all grains, *a*-axis-oriented grains, and *c*-axis-oriented grains of five SBTN samples.

	Sample A	Sample B	Sample C	Sample D	Sample E
All grains (μm ²)	0.04	0.06	0.13	0.19	0.22
<i>a</i> -axis-oriented grains (μm ²)	0.03	0.05	0.05	0.05	0.08
<i>c</i> -axis-oriented grains (μm ²)	0.06	0.07	0.15	0.19	0.26

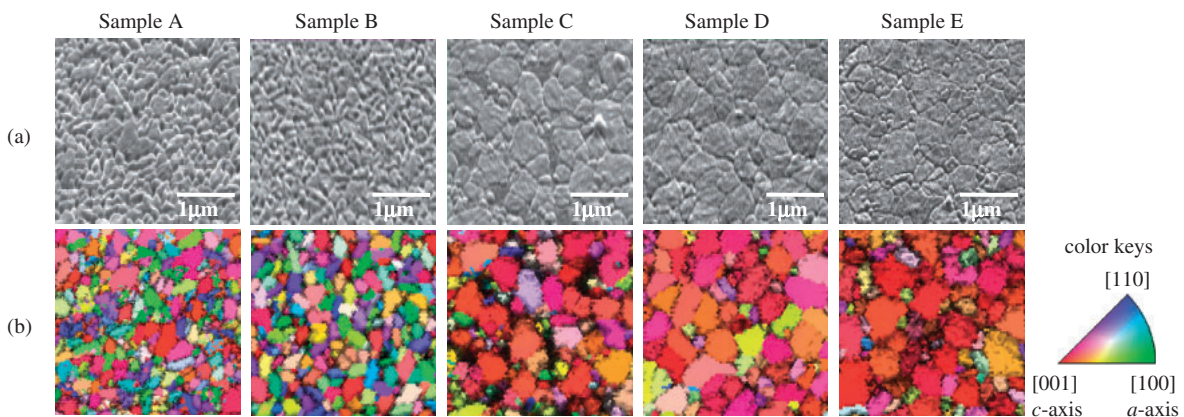


Fig. 2. (a) SEM photographs of SBTN films and (b) their crystal orientation maps defined using EBSD patterns. Samples A to E were prepared by varying the annealing conditions to change the grain size. Samples were labeled from A to E according to the average grain sizes shown in Table I.

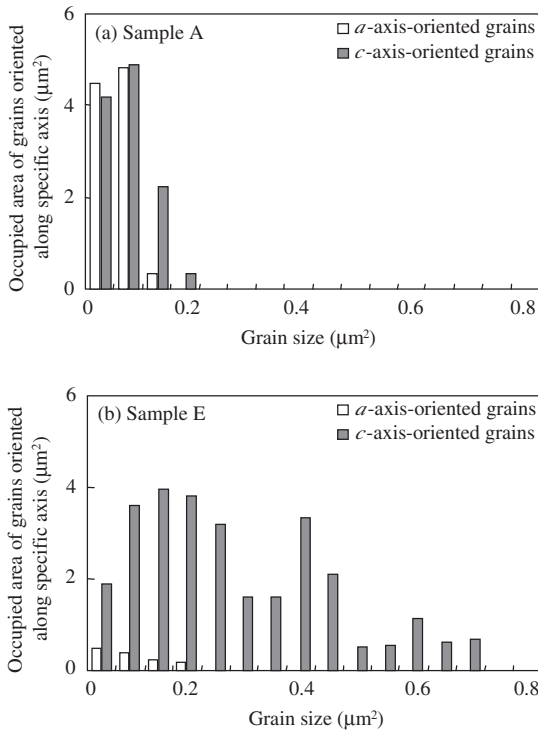


Fig. 3. Occupied areas of *a*- and *c*-axis-oriented grains for (a) Sample A and (b) Sample E as functions of grain size.

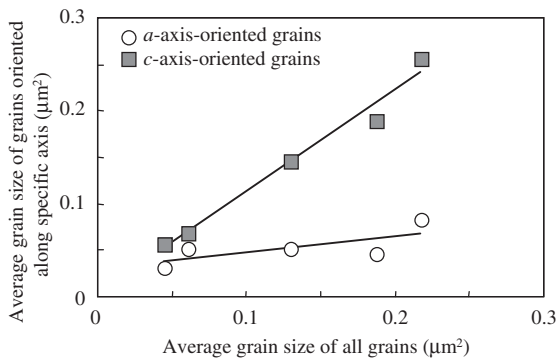


Fig. 4. Average size of grains oriented along specific axis as function of average grain size of all grains.

The average sizes of the *a*- and *c*-axis-oriented grains are determined and plotted as functions of the average size of all the grains for the five samples, as shown in Fig. 4. This result implies that the *c*-axis orientation is dominant in the sample with large grains.

In addition, we measured the polarization versus electric field (*P*–*E*) hysteresis curve of the samples to evaluate the relationship between the crystal orientation and the polarization, as shown in Fig. 5. We also measured the electrical characteristics using a ferroelectric test system operating in the virtual ground mode by applying electric fields up to ± 300 kV/cm. The observed hysteresis curve strongly depends on the grain size. The relationship between the remnant polarization and the average grain size is shown in Fig. 6, in which the remnant polarization of the film increases as the average grain size decreases since the *a*-axis-oriented grain is dominant.

In addition to the top-view analysis of the crystal orientation and size of the grains in the SBTN film, we

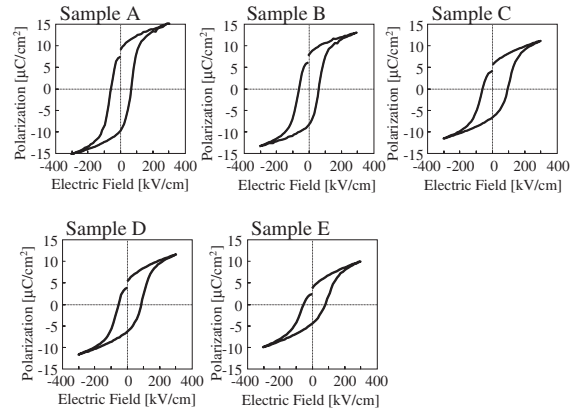


Fig. 5. *P*–*E* hysteresis curves for Samples A to E measured at 60 Hz.

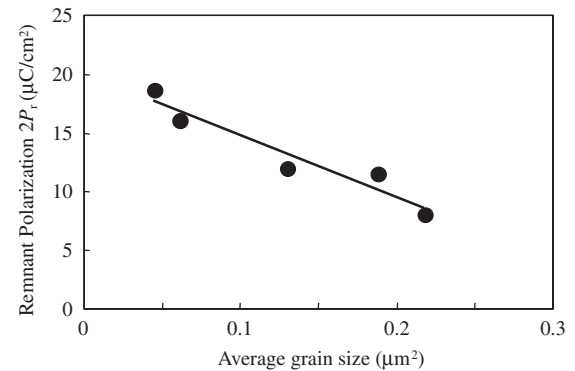


Fig. 6. Remnant polarization $2P_r$ as function of average grain size.

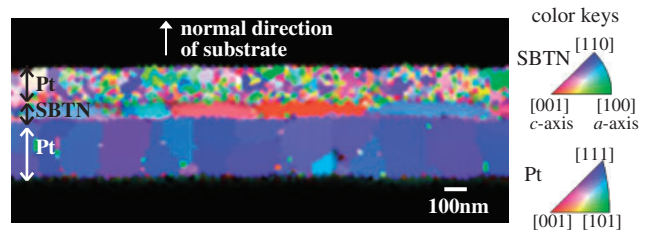


Fig. 7. Cross-sectional crystal orientation map of Sample A with SBTN thickness of 60 nm.

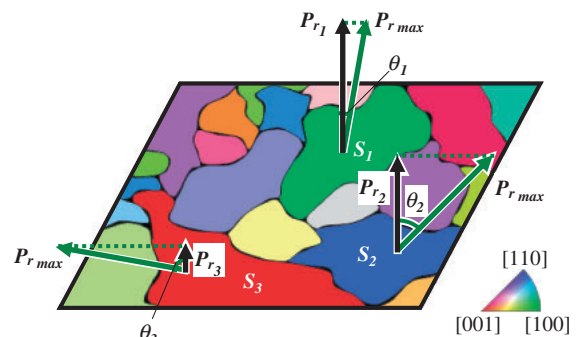


Fig. 8. Schematic illustration for extraction of polarization normal to substrate from individual grains.

conducted the cross-sectional analysis of the Pt/SBTN/Pt structure to evaluate the effects of the crystal orientation and size of the grains in the underlying Pt layer. Figure 7 shows the resultant cross-sectional crystal orientation map

of Sample A. The grains of the Pt layer are also shown in the same figure. The EBSD analysis allows simultaneous measurement for all the three axes without any change in the normal orientation of the sample, because the EBSD patterns show angular relationships in the entire crystal. The principle is similar to that of X-ray pole figure analysis. Thus, the crystal orientation of the normal direction of the sample substrate can also be determined from the results of the cross-sectional EBSD analysis. The obtained result indicates that the resultant ferroelectric grains are grown without being affected by the crystal orientation and size of the Pt grains.

4. Discussion

To analyze the variation in remnant polarization in Samples A to E quantitatively, we calculated the remnant polarizations from the crystal orientation maps in Fig. 2(b) as follows. As shown in Fig. 8, when we consider a grain whose a -axis points a direction along a vector making an angle of θ_i with the normal direction of the substrate, the contribution from the maximum remnant polarization of the grain to the remnant polarization along the normal direction of the substrate is given by $S_i \cos \theta_i / S$, where i is an integer from 1 to n , n is the number of grains observed in the sampled area, S_i is the area of the i -th grain, and S is the sampled area. Here, the size and crystal orientation of each grain are considered, while the effect of each parameter cannot be distinguished. Since the crystal structure is assumed to be tetragonal in this EBSD analysis, the contribution of 90° domain or domain switching is not considered. In this case, the c -axis-oriented grain plays only as a dielectric, which is reflected in the above equation. The total remnant polarization of the entire area along the normal direction of the substrate is calculated to be $\sum_{i=1}^n S_i \cos \theta_i / S$. We can estimate the total remnant polarizations by using the angle θ_i calculated from the crystal orientation and grain size S_i of the i -th grain, which are known from the crystal orientation maps shown in Fig. 2(b).

Figure 9 shows the remnant polarization obtained from hysteresis measurements versus the total polarizations determined from the EBSD results, indicating a good correspondence. The inclination of $2P_r$ for Samples D and E in which the c -axis orientation is dominant is reasonable because the c -axis can be considered only as a dielectric. We can conclude that the remnant polarizations obtained from the hysteresis measurements strongly depend on the distribution of the orientation of the grains. This also implies that we can predict the polarization along the normal direction of the substrate from the EBSD data by only observing the crystal orientation of an SBTN surface without measuring the electrical characteristics of the capacitors.

The above-mentioned results indicate that it is better for a small grain to have a large polarization. In addition, the grain size and crystal orientation of the underlying Pt layer negligibly affect the polarization of the SBTN film over the Pt layer. A better growth technique for distributing the crystal orientation uniformly would also be required for the fabrication of high-density FeRAMs.

The presented EBSD technique would be useful for the design of future high-density FeRAMs since it does not require the fabrication of capacitors to know the total polarization.

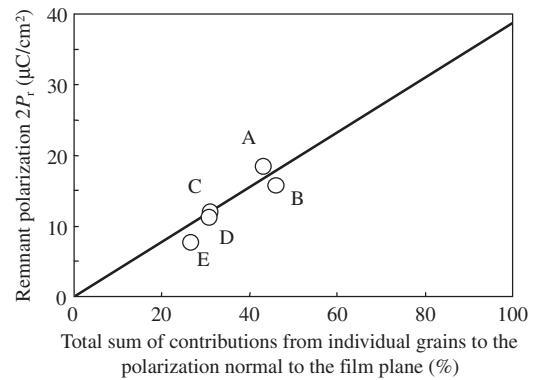


Fig. 9. Remnant polarization measured using P - E hysteresis curves as function of total sum of polarization normal to substrate from individual grains.

The EBSD can be conducted for the cross-sectional analysis as shown in this paper; thus, this technique can also be applied to the design of a 3D capacitor that can make the unit cell much smaller.

5. Conclusions

We investigate the distributions of the size and crystal orientation of individual grains of SBTN films using EBSD patterns for the first time. It is experimentally found that the c -axis orientation is dominant in the sample with a large average grain size. The sample with a small grain size exhibits a more random crystal orientation distribution than the sample with a large grain; thus, more a -axis-oriented grains exist in it. As a result, the remnant polarization is larger in the sample with a small grain, which is also confirmed by P - E hysteresis curve measurement. The cross-sectional analysis of the EBSD patterns indicates that the size and crystal orientation of the grains in the SBTN films are not affected by those of the underlying Pt layer. The presented EBSD technique would be useful for the design and fabrication of future high-density FeRAMs, which may include 3D capacitors.

Acknowledgments

The authors gratefully acknowledge Dr. Daisuke Ueda for instructive suggestions and encouragement throughout this work. They would also like to thank Tetsuzo Ueda for reviewing our manuscript. This work was supported in part by the New Energy and Industrial Technology Development Organization (NEDO) in Japan.

- 1) J. F. Scott and C. A. Paz de Araujo: *Science* **246** (1989) 1400.
- 2) D. J. Taylor, R. E. Jones, P. Zurcher, P. Chu, Y. T. Lii, B. Jiang, and S. J. Gillespie: *Appl. Phys. Lett.* **68** (1996) 2300.
- 3) Y. Shimakawa, Y. Kubo, Y. Nakagawa, T. Kamiyama, H. Asano, and F. Izumi: *Appl. Phys. Lett.* **74** (1999) 1904.
- 4) C. Bae, J. K. Lee, S. H. Lee, and H. J. Jung: *J. Vac. Sci. Technol. A* **17** (1999) 2957.
- 5) B. I. Seo, N. J. Park, S. J. Kim, Y. H. Oh, B. Yang, and S. K. Hong: *J. Korean Phys. Soc.* **45** (2004) 1313.
- 6) A. J. Schwartz, M. Kumar, and B. L. Adams: *Electron Backscatter Diffraction in Materials Science* (Plenum, New York, 2000) p. 1.
- 7) B. L. Adamus, S. I. Wright, and K. Kunze: *Metall. Trans. A* **24** (1993) 819.
- 8) G. Fox, T. Maitland, X. Han, and M. Vaudin: *Proc. Int. Symp. Integrated Ferroelectrics, Korea, 2004*, 10-10-C.